

# Nanoparticle metrology in sol-gels using multiphoton excited fluorescence

J Karolin, C D Geddes, K Wynne and D J S Birch<sup>1</sup>

Photophysics Research Group and Femtosecond Research Centre, Department of Physics and Applied Physics, Strathclyde University, Glasgow G4 0NG, UK

E-mail: DJS.Birch@Strath.ac.uk

Received 10 September 2001, accepted for publication 25 October 2001

Published 23 November 2001

Online at [stacks.iop.org/MST/13/21](http://stacks.iop.org/MST/13/21)

## Abstract

We have developed a method of measuring the growth of nanoparticles during sol-gel glass formation based on labelling the particle with a fluorescent dye and determining the multiphoton excited decay of fluorescence anisotropy due to Brownian rotation. Multiphoton excitation is shown to give a higher dynamic range of measurement than one-photon excitation. We illustrate the sub-nanometre resolution and stability of our approach by detecting a 0.8–1.1 nm silica particle hydrodynamic mean radius increase in a tetramethylorthosilicate sol at pH 2.3 labelled with rhodamine 6G and observed over  $\approx 4$  weeks and also with a stable silica colloid of radius 6 nm, pH 8.9, labelled with a 6-methoxyquinoline-type dye.

**Keywords:** particle metrology, fluorescence anisotropy decay, multiphoton excitation, sol-gel, TMOS

## 1. Introduction

The measurement of particle size in colloids is an important area of metrology, though one which can be difficult because nanometre resolution is frequently required. One range of colloids of great industrial and research interest are those which produce the many types of sol-gel glasses, of which silica gel is probably the best known.

Sol-gel glasses find many important applications ranging from every day applications of silica gel in cleaning, polishing, brewing, printing and adhesive agents to scientific applications in photonics, sensors and chromatography. One of the many mysteries of the sol-to-gel transition is how the properties of the sol including its kinetics translate into the gel at the molecular level. For example, the pore volume and surface area of the final gel determine the performance of the final product and are directly related to the silica particle size which in turn depends on overlapping kinetic processes.

The silica sol-gel process is a room-temperature either organic or inorganic polymerization, whereby the precursor solution ‘the sol’ changes into a rigid network, ‘the gel’, at a rate which is strongly pH and SiO<sub>2</sub> concentration dependent [1]. For hydrogels at pH < 2 (acid catalysed) gelation occurs by means of a series of monomer and/or

inter-cluster condensation reactions between silanol (–Si–OH) bonds to form ramified siloxane (–Si–O–Si–) clusters. At pH > 8 (base catalysed) more solid siloxane based particles can grow larger by monomer addition as smaller particles dissolve (Ostwald ripening), or by aggregation. At intermediate pH values of 3–7 both growth mechanisms, under certain conditions, can be observed. Silica gels can typically be produced by two main methods, i.e. the hydrolysis and polycondensation of either lithium, sodium or potassium silicates, either acid or base catalysed (an *inorganic* polymerization), or from acid or base catalysed tetrafunctional alkoxides (an *organic* polymerization). The former gels are frequently referred to as hydrogels and the latter as alcogels in accordance with both the solvents used and condensed.

Traditionally, small-angle scattering of laser light, x-rays or neutrons has been used to study silica particle growth. For example, light scattering measurements on an alkoxide-based sol found a primary particle hydrodynamic diameter of 1.0 nm increasing to 2.4 nm prior to gelation [2]. Small-angle x-ray scattering studies of silica gel have revealed evidence for 1 nm particles [3] and similar studies on another alkoxide sol indicate that 2 nm diameter primary particles aggregate to form secondary particles of 6 nm diameter prior to gelation [4]. Small angle neutron scattering has found comparable primary particle dimensions [5]. In one

<sup>1</sup> Corresponding author.

of the few studies on silica hydrogel formation, primary particles of  $\approx 1$  nm have been detected using small-angle x-ray scattering [6]. However, scattering methods have a number of drawbacks. For example, they need low silicate and therefore low final  $\text{SiO}_2$  (w/w) concentrations to avoid multiple scattering and sol or precursor solution dilution is not the answer, as this can cause depolymerization in aqueous-based systems or even *back* hydrolysis in alkoxide derived gels [1]. Moreover, scattering by the gel matrix after the sol-to-gel transition at a time  $t_g$  corrupts the particle scattering measurement. X-ray and neutron scattering in particular are also very expensive and unsuitable for on-line use. Light scattering is limited in resolution by the wavelength of light and electron microscopy can only be used on dry colloids.

Fluorescence correlation spectroscopy [7] and fluorescence recovery after photobleaching [8] possess sufficient resolution for silica particle metrology, but also suffer from the need to dilute the sols and have the added complication of requiring a microscope.

Recently we have reported the use of one photon excited fluorescence anisotropy decay with nanosecond resolution to determine the growth in hydrodynamic radius of silica particles in a hydrogel over the range  $\sim 1.5$ – $4.5$  nm at pH  $\sim 1$  [9, 10]. Although fluorescence anisotropy decay has been widely used in biochemistry to determine structure and dynamics in membranes and proteins [11] it has hitherto found little if any application where the hydrodynamic radius of the fluorescing rotor species changes with time. Nevertheless our results show that fluorescence anisotropy decay overcomes many of the drawbacks of scattering methods. For example, because in the absence of energy migration fluorescence anisotropy will decay only by particles rotating, we can investigate particles at higher silicate concentrations and even after gelation has occurred. Similarly, although multiphoton excited fluorescence is finding increasing use in biochemical systems [12] it has not hitherto been used in particle metrology.

Here we demonstrate the additional benefit in terms of reduced Rayleigh scattering and higher resolution achievable when using femtosecond multiphoton excitation in the near infrared and resolve the particle growth in a tetrafunctional alkoxide derived sol for the first time using fluorescence.

## 2. Theory

A multiphoton process originates when a molecule is excited to a higher electronic state by absorbing two or more photons in the same quantum event. In multiphoton excitation the fluorescence intensity  $I_{fl}$  does not increase proportionately with increasing excitation power density  $\rho_{exc}$ , but follows the relationship [12]

$$I_{fl} = \gamma(\phi_{fl}/i)n d\sigma_i\rho^i \quad (1)$$

where  $\gamma$  is a fluorescence collection efficiency factor,  $\phi_{fl}/i$  the one-photon excited fluorescence quantum yield corrected for the multiphoton absorption,  $n$  the number density of absorber,  $\sigma_i$  the absorption cross section for  $i$  photons and  $d$  the sample path length. Equation (1) shows that in principle the gradient of a simple log–log plot of experimentally measured  $I_{fl}$  and  $\rho$  values allows  $i$ , the number of photons absorbed, to be determined.

Vertically and horizontally polarized fluorescence decay curves,  $F_V(t)$  and  $F_H(t)$ , of relative transmission  $g$  and orthogonal to vertically polarized excitation recorded at different delay times following initial mixing of the sol lead to an anisotropy function  $R(t)$  describing the rotational correlation function where

$$R(t) = \frac{F_V(t) - gF_H(t)}{F_V(t) + 2gF_H(t)}. \quad (2)$$

Previous analysis of  $R(t)$  for silica hydrogels showed that the best description was provided by two rotational correlation times  $\tau_{r1}$  and  $\tau_{r2}$  in the form [9, 10]

$$R(t) = (1 - f)R_0 \exp(-t/\tau_{r1}) + fR_0 \exp(-t/\tau_{r2}) \quad (3)$$

where  $R_0$  is the initial anisotropy,  $f$  the fraction of fluorescence due to probe molecules bound to silica particles and hence  $1 - f$  the fraction due to free dye in the sol. (Further terms can be added, if appropriate, to include other dye locations, e.g. dye trapped in the gel.) From the Stokes–Einstein relation  $\tau_{r1}$  gives the sol microviscosity,  $\eta = 3\tau_{r1}kT/4\pi r^3$  where  $r$  is the hydrodynamic radius of the dye and likewise using  $\eta$  and  $\tau_{r2}$ , the average silica particle hydrodynamic radius is obtained.

One important difference with our previous one-photon excitation studies [9, 10] concerns the higher degree of molecular orientation photoselected and associated increase in the initial value of the fluorescence anisotropy,  $R_{0i}$ , when using polarized multiphoton excitation. For multiphoton excitation a higher degree of orientation of molecules is required at  $t = 0$  according to a directional distribution function  $f_i(\theta)$ , which can be approximated for the case of cylindrical symmetry and a dominant transition tensor to be [13]

$$f_i(\theta) = \cos^{2i} \theta \quad (4)$$

where  $\theta$  is the angle between the plane of polarization of excitation and the absorption transition dipole moment. This increasing degree of photo-selection with  $i$  can also be expressed as [13]

$$R_{0i} = \frac{2i}{2i+3} \left[ \frac{3}{2} \cos^2 \beta_i - \frac{1}{2} \right] \quad (5)$$

where  $\beta_i$  describes the intramolecular angle between the dominant absorption and emission transition moments. Equation (5) describes the maximum dynamic range of anisotropy measurement which, in the collinear ( $\beta_i = 0$ ) case, is  $R_{0i} = 0.4$  for  $i = 1$ ,  $0.57$  for  $i = 2$  and  $0.67$  for  $i = 3$ . This increase in initial anisotropy facilitated by multiphoton excitation is potentially very useful when resolving complex rotational kinetics (i.e. more than one rotational correlation time).

## 3. Instrumentation and methods

Figure 1 shows the femtosecond fluorometer we have used for particle metrology. It is based on time-correlated single-photon counting detection [14] and multiphoton excitation provided by femtosecond pulses from a Ti:sapphire laser system. It contains a number of improvements over the instrument we reported previously [15], most notably in

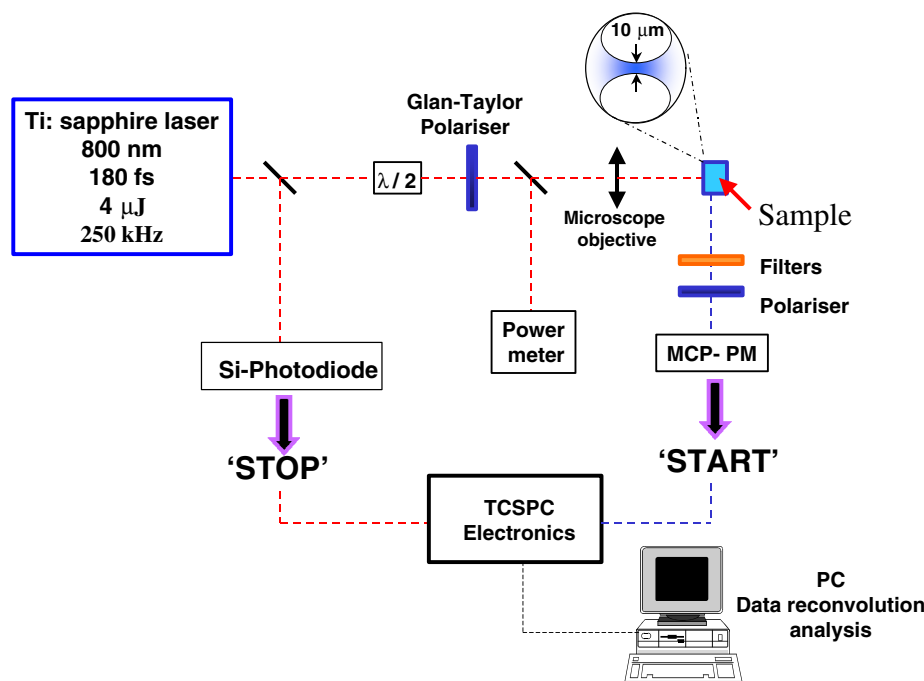


**Figure 1.** Fluorometer for nanoparticle metrology based on multiphoton excitation using femtosecond laser pulses and time-correlated single-photon counting detection.

(This figure is in colour only in the electronic version)

respect of a faster single-photon timing discriminator and microchannel plate photomultiplier [16]. The system not only permits the measurement of fluorescence lifetimes, but also time-resolved and time-integrated fluorescence emission spectra, fluorescence anisotropy decay and fluorescence dependence on laser power (cf equation (1)) all using both multiphoton and frequency-doubled one-photon excitation.

Excitation is provided by 250 kHz regeneratively amplified Ti:sapphire (coherent) laser pulses of duration  $\sim 120$  fs and energy  $\sim 4 \mu\text{J}$  at 800 nm. The linearly polarized laser pulse is passed through a quartz half-wave plate ( $\lambda/2$ ) and a Glan–Taylor polarizer which together enable the laser power falling on the sample to be varied without influencing the pulse duration. The excitation power density was increased beyond the multiphoton threshold using a 1 cm diameter microscope objective ( $f = 73.5$  mm,  $\text{NA} = 0.05$ ) to produce a diffraction limited focus of  $\sim 10 \mu\text{m}$  diameter giving a maximum flux density of  $\sim 10^{31}$  photons  $\text{cm}^{-2} \text{s}^{-1}$ . Negligible depolarization is introduced by this lens, as evidenced by the measured  $R_0$  values being close to the theoretical values, i.e. 0.38 for one-photon excitation of DPH, 0.50 for two-photon excitation of rhodamine 6G and 0.64 for three-photon excitation of p-terphenyl [15]. Note from equation (3) that  $R_0$  cancels out when determining  $f$  and the rotational times are independent of  $f$  and  $R_0$ .

Care was taken to recognize and avoid associated effects of working at high power densities such as photolysis, photobleaching, excited state absorption, second harmonic or white light generation in a quartz cuvette, self-focusing, dielectric breakdown, stimulated emission etc [12]. The main adjustments being the laser wavelength, power density and depth of focus. Consistent with previous work [12] no evidence for a reduction in rotational times due to temperature increase

under multiphoton excitation conditions was found. The white light continuum provided by a sapphire glass plate was used in conjunction with a 500 nm interference filter for obtaining the one-photon excitation of rhodamine 6G. Judicious use of 1 mm apertures confines the detected fluorescence signal to the region of maximum multiphoton excitation and minimizes spatial time-spread and scattered light detection.

Multiphoton excited fluorescence was wavelength selected by means of a 800 nm cut-off filter to exclude the laser fundamental and for one-photon excitation of rhodamine 6G a 550 nm long-pass filter was employed. A Glan–Taylor prism polarizer in this channel permitted both magic angle ( $54.7^\circ$ ) measurements for obtaining fluorescence decay curves, undistorted by rotation and anisotropy measurements when automatically toggled between vertical and horizontal polarizations to average out the effect of laser intensity drifts. The g-factor was found to be unity. A microchannel plate photomultiplier (Hamamatsu R3809U-50) was used for detection. Standard single-photon timing NIM electronics are complimented with a EG&G Ortec close-coupled Model 9327 1 GHz amplifier and timing discriminator. The overall instrumental response function, as recorded by scatter of the excitation light using Ludox in the sample cell, was  $\sim 100$  ps full width at half maximum (fwhm). The biased time-to-amplitude converter (Ortec 457) was operated in reverse mode [14], laser pulse ‘stop’ synchronization being obtained by splitting the laser beam and detection with a Si-photodiode (BPX 65,  $-9$  V bias, rise-time 3.5 ns). The order of multiphoton absorption was determined using an optical power meter (Newport Model 835) to monitor the laser and an analogue rate meter to monitor the fluorescence photons. Both signals are digitized and data collected simultaneously under software control of the excitation half-wave plate [15]. Fluorescence and anisotropy decay parameters are

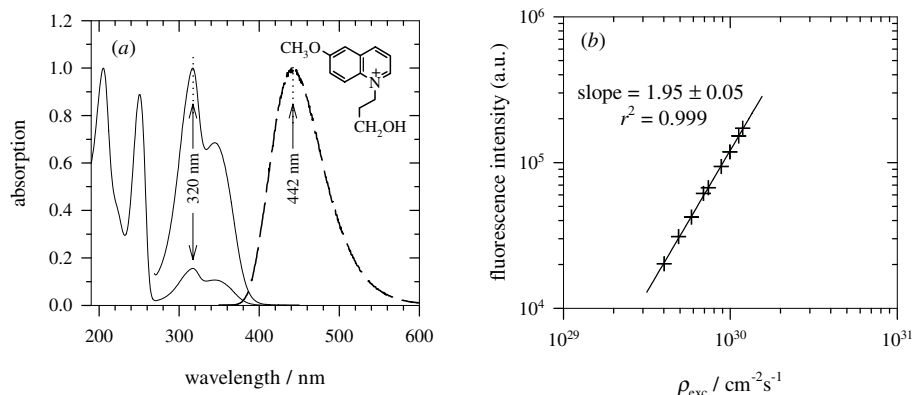


**Figure 2.** (a) Absorption (—) and emission (---) spectra of a  $10^{-5}$  M solution of CG437 in  $H_2O$ . The absorption spectrum in the region 280–400 nm is expanded for clarity. Inset—molecular structure of CG437. (b) Log–log plot of fluorescence intensity dependence of CG437 labelled silica particle (AM30) on the incident photon flux density at 800 nm. The regression coefficient is denoted  $r$ .

obtained using nonlinear least-squares reconvolution analysis (IBH software).

Tetramethylorthosilicate (TMOS) based sol-gels were made by mixing TMOS, ethanol, water (doubly deionized) and HCl together to produce pH 2.3, 21.91% (w/w)  $SiO_2$  sol-gels. A concentrated ethanol stock solution of rhodamine 6G was used in the preparation to adjust the optical density of the sol to less than 0.1 at  $\lambda_{abs\ max} = 530$  nm.  $3.5\ cm^3$  of sol was then cast into quartz cuvettes and sealed. For all measurements the samples remained optically transparent such that depolarization due to multiple scattering from particles and pores could be neglected. The gelation time,  $t_g$ , was 56 160–59 040 min at  $\approx 20^\circ C$ . A Ludox colloidal silica (Du Pont’s AM30, 30% w/w  $SiO_2$ , 6 nm radius, pH 8.9) was labelled with CG437, a 6-methoxyquinoline-type dye that we have recently synthesized for this purpose [17]. For CG437 one-photon excitation was provided at 370 nm by means of nanosecond pulses from an IBH NanoLED operating at 1 MHz and at 400 nm by the femtosecond frequency-doubled Ti:sapphire laser.

## 4. Results and discussion

### 4.1. Choice of dye

The choice of dye for labelling the particles is crucial and is influenced by several criteria. Ideally a dye should have a fluorescence lifetime which is comparable to the rotational correlation time of the particle [11, 14] and constant when the dye is free in the sol and when bound to the particle. The dye should be stable at the pH used, have a good quantum yield (say  $>0.2$ ), a high multiphoton absorption cross section and collinear absorption and emission transition dipoles, i.e.  $\beta_i = 0$  in order to maximize  $R_0$  (cf equation (5)). Minimizing the dye size in comparison to the particle is also important. The dye should be water or alcohol soluble depending on the gel. Although functionality of the dye can be achieved to ensure covalent attachment to the silica [18], our experience is that other mechanisms, for example coulombic attraction, are often adequate. The isoelectric point and the point of zero charge of silica are in the pH range  $\approx 1-3$  [1] and therefore both anionic and cationic dyes have their uses. Inevitably a compromise

in the choice of dye is usually necessary. The merits of rhodamine 6G are that it is stable over a wide pH range, highly fluorescent, has a high two-photon absorption cross-section [19,20], is readily taken up by silica, has a fluorescence lifetime of  $\approx 4$  ns, which is compatible with nanometre particle rotational times in the sols studied and  $R_{02} \sim 0.57$ . CG437 is cationic (charge balanced with a bromide counter-ion) and has solvent-dependent bi-exponential fluorescence lifetimes of  $\approx 10-28$  ns [17] making it more suitable than rhodamine 6G for studying particles of a 10 nm scale, but gives  $R_{01}, R_{02} < 0.4$  implying  $\beta_i \neq 0$ .

Figure 2(a) shows the one-photon absorption and fluorescence spectra of an aqueous solution of CG437 and its molecular structure. Figure 2(b) shows the laser power dependence of the fluorescence intensity for CG437 labelled Ludox AM30. The slope obtained supports the presence of two-photon excitation (cf equation (1)). It has also been shown previously that rhodamine 6G undergoes two-photon excitation when excited at 800 nm [15]. It is interesting to note that the obvious step of frequency doubling the Ti:sapphire laser to obtain one photon excitation of rhodamine 6G at 400 nm results in an unworkably low  $R_{01}$  value [15].

### 4.2. Sol-gel particle growth (dynamic nanoparticle metrology)

Figure 3 shows the measured polarized fluorescence decay curves  $F_V(t)$  and  $F_H(t)$  and the derived anisotropy decay  $R(t)$  for the TMOS sol using two-photon excitation at 800 nm.  $R(t)$  obtained from one-photon excitation ( $\approx 500$  nm) using part of the white light continuum generated around 800 nm is shown for comparison. One of the advantages of the measurement technique we have developed is that equation (3) also gives the microviscosity of the sol as well as the particle mean radius. For the TMOS sol we found the fraction of fluorescence  $f$  due to dye bound to the particles remained constant at  $\approx 30\%$  during the polymerization. Rhodamine 6G is taken up very efficiently by silica, so on this evidence alone we cannot rule out the possibility that in fact all the dye is taken up and that the ‘free’ dye rotation ( $1 - f$  in equation (3)) actually refers to dye tethered and wobbling on the particle and  $f$  to the dye rigidly bound. However, on immersing the final gel in

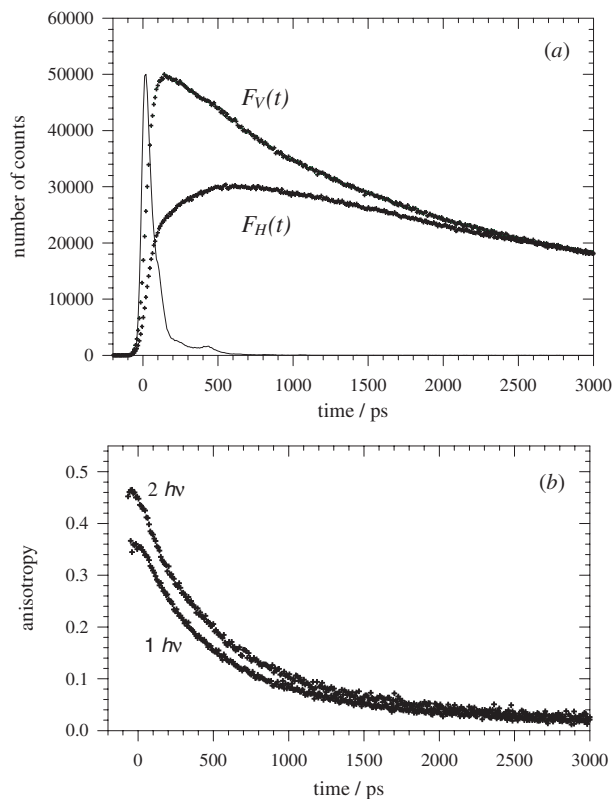


**Figure 3.** (a) Two-photon polarized fluorescence decays and instrumental response function and (b) corresponding one- and two-photon anisotropy decays  $R(t)$  for the TMOS sol-doped with rhodamine 6G at 41 663 mins. The channel width is 8.7 ps.

ethanol a fraction of dye diffuses out and not all the dye can be washed out, implying that not all the dye is trapped. Also,  $\tau_{r1}$  is  $\sim 300$  ps, i.e. compatible with that for the free dye in the water/alcohol mixture we have in the sol and for the purpose of calculating the hydrodynamic mean radius the model given by equation (3) is independent of these alternative interpretations of  $f$ . Here we have used the viscosity determined from  $\tau_{r1}$  assuming the theoretical hydrodynamic radius for rhodamine 6G of 0.56 nm [21]. Our own study of rhodamine 6G in a range of known viscosity solvents gave a hydrodynamic radius of  $0.53 \pm 0.03$  nm which is consistent with other work, for example 0.54 nm [22] and  $0.60 \pm 0.04$  nm [23]. If the dye is tethered and wobbling on the particle then it will be reporting a vicinal microviscosity, which is not necessarily the same as that encountered by the particle. The bulk viscosity and sol microviscosity are also likely to be quite different. Fortunately, since  $r \sim \eta^{-3}$  the viscosity value is less critical.

Figure 4 shows how the calculated viscosity and particle mean radius change with polymerization time, pt. The viscosity values are similar in magnitude and show a slight downward trend with time, similar to what we observed previously for a silica hydrogel [9, 10], reflecting here the polymerization of the sol and the expulsion of methanol. In many respects it is a misnomer to refer to the silica clusters as particles, which implies a solid morphology and not the ramified structure with a distribution of sizes, which is likely to be encountered. Also, the dye, if not fully intercalated, will contribute to the measured particle size. Nevertheless, at the pH chosen of 2.3 the sol is *slow gelling* such that the silica

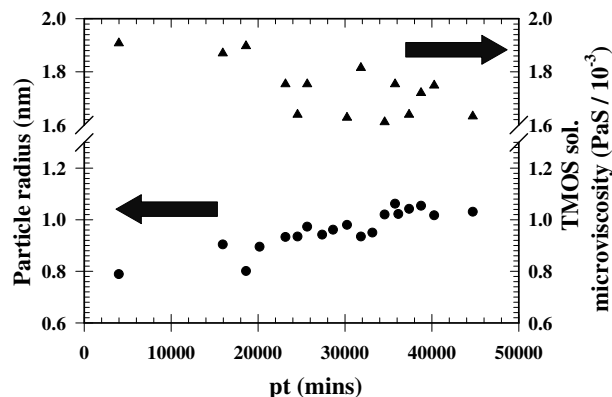


**Figure 4.** Silica particle radius, ●, and sol microviscosity, ▲, as a function of polymerization time, pt, for the TMOS sol. The errors in particle radius were typically  $\pm 0.1$  nm.

**Table 1.** Silica particle radii determined using one and two photon excitation on the TMOS sol as a function of polymerization time.

pt (min)	Particle radius (nm)	
	1 $h\nu$	2 $h\nu$
1 263	0.82	0.74
2 775	0.78	0.81
11 400	0.85	0.82
24 360	0.88	0.90
41 663	0.95	0.93

Note: The microviscosity,  $\eta$ , used in particle size determination was calculated using  $\tau_{r1}$  and the Stokes–Einstein equation,  $\eta = 3\tau_{r1}KT/4\pi r^3$ , with a rhodamine 6G radius of 5.6 Å. The pt values for 1 and 2  $h\nu$  measurements are the mean values of both times, where measurements were typically of <30 min duration.

particles undergo negligible growth by aggregation during the measurement, even during the long measurement times needed to obtain high statistical precision (typically 30 min). This has enabled us to observe the very early stages of polymerization at a high resolution of  $< 1$  nm, i.e. as good as, if not better than any scattering technique and with the additional advantages of being able to work at high silicate concentrations beyond  $t_g$  and obtain molecular viscosity information. Previously we fitted the growth of silica hydrogels using  $r \sim 1 - e^{-kt}$  and attributed this to particle–particle aggregation [9, 10]. Here figure 4 can clearly be approximated by  $r \sim kt$ , reflecting the different growth mechanism associated with monomer–monomer and monomer–particle addition in TMOS under these conditions [1].

Table 1 compares the particle mean radii determined using one- and two-photon excitation on the TMOS sol as a function of pt. The results show no evidence of a systematic discrepancy (e.g. due to heating under two-photon conditions) and are consistent given that pt is slightly different for the one and two-photon measurements, which were in fact taken sequentially.

#### 4.3. Stable colloid (static nanoparticle metrology)

In order to check the range of particle sizes, which could be measured and compared with well-characterized colloids, we studied a Du Pont Ludox colloid labelled with CG437,

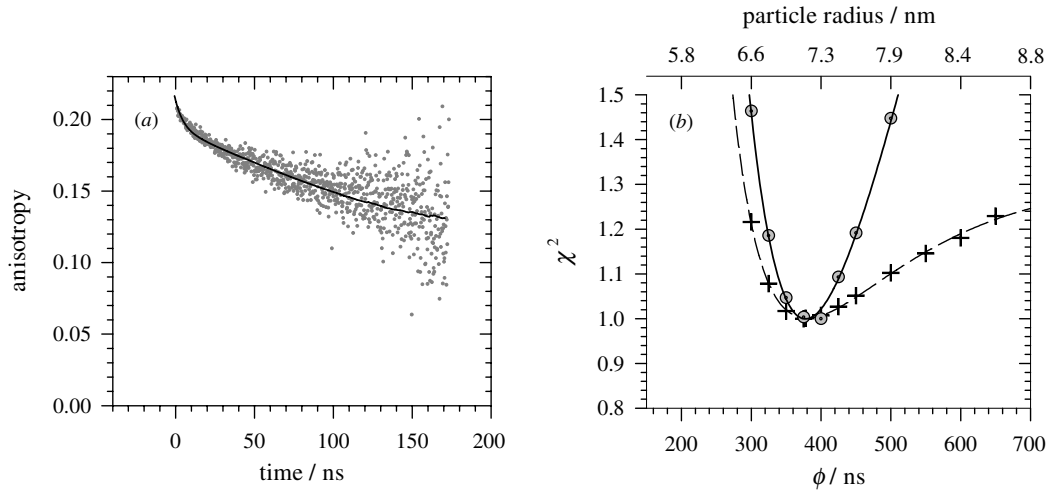


**Figure 5.** (a) Two-photon induced fluorescence anisotropy decay of Ludox AM30 particles labelled with CG437 ( $\lambda_{\text{exc}} = 800$  nm). The corresponding number of counts in the difference curve, i.e. the numerator in equation (2), is  $\approx 50\,000$  and the time per channel is 193 ps. (b)  $\chi^2$  analysis of the anisotropy data given in (a) (+) and synthetic data (O) generated for a normal distribution of  $7.2 \pm 0.1$  nm particles undergoing Brownian rotational diffusion. The minimum of the  $\chi^2$  curve has been normalized to unity for comparison.

**Table 2.** Silica particle radii determined using one-(400 and 370 nm) and two-(800 nm) photon excitation. The manufacturer's value for Ludox AM30 is 6 nm.

Sample	Fluorescence decay parameters				Anisotropy decay parameters				
	$\lambda_{\text{exc}}$ (nm)	$\tau_1, \tau_2$ (ns)	%	$\chi^2$	$R_0$	$\tau_r$ (ns)	%	$\chi^2$	Particle radius (nm)
AM30	800	$12.6 \pm 1.20$	21	1.18	0.219	$375 \pm 90$	90	1.11	7.13
		$31.5 \pm 0.63$	79			$5.0 \pm 4.8$	10		
AM30	400	$14.0 \pm 0.80$	14	1.16	0.276	$431 \pm 84$	95	1.02	7.47
		$33.6 \pm 0.78$	86			$4.2 \pm 10.0$	5		
AM30	370	$8.5 \pm 0.12$	41	1.2	0.250	$434 \pm 69$	100	1.09	7.48
		$25.4 \pm 0.14$	59						

Note: A microviscosity of  $10^{-3}$  PaS was used in the particle radii determination. For femtosecond two-photon 800 nm, frequency-doubled 800 to 400 nm and 370 nm IBH NanoLED nanosecond excitation, the channel width was  $\approx 191$  ps.

namely Ludox AM30. The particles in Ludox are discrete uniform spheres of silica, which have no internal surface area or detectable crystallinity. The 6 nm radius particles are dispersed in a pH 8.9 alkaline medium (NaOH), which reacts with the silica surface to produce a negative surface charge, balanced with sodium ions. In addition, some of the surface silicon atoms have been replaced with aluminium atoms, which creates a fixed negative charge, independent of pH, affording particle stability over the alkaline range. Because of the negative surface charge the particles repel one another resulting in stable colloids, which is ideal to test the validity of our approach. Table 2 compares the measured radii for one- and two-photon excitation ( $\sim 7$  nm) and the manufacturer's value ( $\sim 6$  nm) as reported on the Ludox data sheet. The  $\sim 1$  nm difference may well reflect the influence of bound water on the hydrodynamic radius which we measure and indeed the contribution of the probe dimensions. Moreover, the Du Pont value might refer to the dry colloid. Figure 5(a) shows an anisotropy decay curve we have recorded for silica particle rotation in this colloidal suspension. As can be seen from figure 5(a), an initially rapid depolarization is followed by a slower component. The slower anisotropy decay component ( $\sim 400$  ns) reflects the Brownian rotation of the colloidal particle, but the origin of the faster

component (e.g.  $\sim 5 \pm 4.8$  ns) is unclear. Given the large error it is not possible to identify the fast component, but possible explanations include wobbling of dye molecules tethered to the particle, a distribution of radii, energy migration between dye aggregates on the particle and intramolecular reorientation of the emission dipole. Figure 5(b) shows the  $\chi^2$  analysis of the anisotropy data given in 5(a) (+) and synthetic data (O) generated for a normal distribution of mean radius  $7.2 \pm 0.1$  nm solid silica particles undergoing Brownian rotational diffusion. In the analysis of the real data (+) the weaker and shorter correlation time of  $\approx 5$  ns was allowed to vary freely while the longer and dominating component,  $\approx 95\%$ , was fixed at different values corresponding to different particle size estimates during the least squares minimization of  $\chi^2$ . As can be seen from figure 5(b) the broader  $\chi^2$  surface for the real data as compared to the synthetic data implies that a distribution of particle sizes is present, although this appears relatively narrow. The skewness suggests the size distribution is weighted towards a mean radius  $> 7.2$  nm, the colloid in fact slowly aggregating with time. These observations look promising for the study of either static or dynamic size distributions of particles in general, but such analysis, though beyond the scope of this paper, is under further investigation in our laboratory.

## 5. Conclusions

Fluorescence anisotropy decay offers a realistic alternative to scattering techniques and other methods of particle metrology, particularly when high silicate concentrations are encountered or when studies are required after the gel point. Moreover, the resolution achieved is very high. Multiphoton excitation offers additional capabilities by virtue of the increased dynamic range, which is useful when multiple rotational correlational times are to be detected or when the fluorescence lifetime is much less than the rotational correlation time. Multiphoton excitation is of course achieved at greater expense and increased complexity. The main disadvantage of the approach we have been using lies in the possible obtrusive nature of the fluorescent dye, both hydrodynamically in contributing to the overall radius and chemically and sterically with respect to the sol-gel kinetics. Notwithstanding these factors our results are consistent with a large body of literature on similar sols investigated with scattering techniques [2–6].

Further work comparing our findings with previous fluorescence studies on sol-gels, which have hitherto concentrated on viscosity changes [24], will be reported shortly.

## Acknowledgment

The authors wish to thank EPSRC for research grants.

## References

- [1] Brinkler C J and Scherer G W 1990 *Sol-Gel Science: The Physics and Chemistry of Sol-Gel Processing* (New York: Academic)
- [2] Boonstra A H, Meeuwse T P M, Baken J M E and Aben G V A 1989 A two-step silica sol-gel process investigated with static and dynamic light-scattering measurements *J. Non-Cryst. Solids* **109** 153–63
- [3] Himmel B, Gerber Th and Burger H 1987 X-ray diffraction investigations of silica-gel structures *J. Non-Cryst. Solids* **91** 122–36
- [4] Orcel G, Hench L L, Artaki I, Jonas J and Zerda T W 1988 Effect of formamide additive on the chemistry of silica sol gels 2—gel structure *J. Non-Cryst. Solids* **105** 223–31
- [5] Winter R, Hua D W, Thiyagarajan P and Jonas J 1989 A SANS study of the effect of catalyst on the growth-process of silica-gels *J. Non-Cryst. Solids* **108** 137–42
- [6] Gerber T, Himmel B and Hubert C 1994 WAXS and SAXS investigation of structure formation of gels from sodium-water glass *J. Non-Cryst. Solids* **175** 160–8
- [7] Thompson N L 1991 Fluorescence correlation spectroscopy *Topics in fluorescence spectroscopy: Techniques* vol 1, ed J R Lakowicz (New York: Plenum) pp 337–410
- [8] Birmingham J J, Hughes N P and Treloar R 1995 Diffusion and binding measurements within oral biofilms using fluorescence photobleaching recovery methods *Phil. Trans. R. Soc.* **350** 325–43
- [9] Birch D J S and Geddes C D 2000 Sol-gel particle growth studied using fluorescence anisotropy: an alternative to scattering techniques *Phys. Rev. E* **62** 2977–80
- [10] Geddes C D and Birch D J S 2000 Nanometre resolution of silica hydrogel formation using time-resolved fluorescence anisotropy *J. Non-Cryst. Solids* **270** 191–204
- [11] Steiner R F 1991 Fluorescence anisotropy: theory and applications *Topics in Fluorescence Spectroscopy: Principles* vol 2, ed J R Lakowicz (New York: Plenum) pp 1–51
- [12] Birch D J S 2001 Multiphoton excited fluorescence spectroscopy of biomolecular systems *Spectrochim. Acta A* **57** 2313–36
- [13] Gryczynski I, Malak H and Lakowicz J R 1995 3 Photon induced fluorescence of 2,5-diphenyloxazole with a femtosecond Ti:sapphire laser *Chem. Phys. Lett.* **245** 30–5
- [14] Birch D J S and Imhof R E 1991 Time domain fluorescence spectroscopy using time-correlated single-photon counting *Topics in Fluorescence Spectroscopy: Techniques* vol 1, ed J R Lakowicz (New York: Plenum) pp 1–95
- [15] Volkmer A, Hatrick D A and Birch D J S 1997 Time-resolved nonlinear fluorescence spectroscopy using femtosecond multiphoton excitation and single-photon timing detection *Meas. Sci. Technol.* **8** 1339–49
- [16] Hungerford G and Birch D J S 1996 Single-photon timing detectors for fluorescence lifetime spectroscopy *Meas. Sci. Technol.* **7** 121–35
- [17] Geddes C D, Apperson K and Birch D J S 2000 New fluorescent quinolinium dyes—applications in nanometre particle sizing *Dyes Pigments* **44** 69–74
- [18] VanBlaaderen A and Vrij A 1992 Synthesis and characterisation of colloidal dispersions of fluorescent, monodisperse silica spheres *Langmuir* **8** 2921–31
- [19] Fischer A, Cremer C and Stelzer E H K 1995 Fluorescence of coumarins and xanthenes after two-photon absorption with a pulsed titanium–sapphire laser *Appl. Opt.* **34** 1989–2003
- [20] Albota M A, Xu C and Webb W W 1998 Two-photon fluorescence excitation cross sections of biomolecular probes from 690 to 960 nm *Appl. Opt.* **37** 7352–6
- [21] Porter G, Sadkowski P J and Tredwell C J 1977 Picosecond rotational diffusion in kinetic and steady state fluorescence spectroscopy *Chem. Phys. Lett.* **49** 416–20
- [22] Eichler H J, Klein U and Langhans D 1979 Measurement of orientational relaxation times of rhodamine 6G with a streak camera *Chem. Phys. Lett.* **67** 21–3
- [23] Olivini F, Beretta S and Chirico G 2001 Two-photon fluorescence polarization anisotropy decay on highly diluted solutions by phase fluorometry *Appl. Opt.* **55** 311–7
- [24] Narang U, Wang R, Prasad P N and Bright F V 1994 Effect of aging on the rhodamine 6G in tetramethyl orthosilicate-derived sol-gels *J. Phys. Chem.* **98** 17–22